J. Fluid Mech. (1969), *vol.* 36, *part* 2, *pp.* 385–400
Printed in Great Britain

The onset of cellular convection in a fluid layer with time-dependent density gradients

By L. M. BLAIR AND J. A. QUINN
Department of Chemistry and Chemical Engineering,
University of Illinois, Urbana, Illinois

(Received 11 July 1968)

Onset times for convection induced by buoyancy forces have been measured. Results on three aqueous systems are summarized in terms of a critical value for a time-dependent Rayleigh number. Because of the presence of minute traces of unavoidable surface-active contaminants, a 'free' water surface behaved as if it were inflexible and laterally rigid so far as determining first convective motion was concerned. The form of the onset motion was observed with schlieren photography for both top and side view. The pattern at onset was frequently in the form of plunging rings. Surface effects were demonstrated with an organic liquid layer in which onset times were measured for convection driven by surface tension gradients as well as by buoyancy forces. The data are compared with some recent predictions of linear stability analyses.

1. Introduction

The phenomenon explored in this study is that of the onset of convection in an initially homogeneous horizontal fluid layer. Convection is induced by abruptly changing the temperature (or composition) at the boundary of the layer. If the accompanying transient density gradient is of proper sense and magnitude the layer will be unstable and disturbances will grow. The manifestation of these disturbances, grown to some observable size, is identified as the onset of convection. In this paper we report experimental measurements of onset times and other characteristics of the convective flow. Our results cover a wide range of parameters including both buoyancy and surface-driven flows. Onset times are consistent with some predictions of linear stability theory as are the wavenumbers of the fastest growing disturbances. These first disturbances frequently appear in the form of ring cells—a pattern which, apparently, has not been previously observed.

In recent literature this problem has received considerable attention, both because of its practical significance and because of certain unresolved features of the transient stability analysis. These linear stability analyses have been of two types: those employing the so-called 'quasi-static' assumption (Morton 1957; Lick 1965; Currie 1967) and those in which the time-dependency is treated as an initial-value problem (Foster 1965*a*, 1968; Mahler, Schechter & Wissler 1968). In the former case it is assumed that the growth rate of disturbances is large

compared to the time rate of change of the density gradient and, therefore, at any instant the non-linear profile can be 'frozen' and its intrinsic stability examined. In this way the time-dependency is effectively removed with the result that predictions are independent of initial conditions, i.e. disturbances present at time zero. In the latter approach the full, linearized equations are examined with time-dependent terms retained. The difficulties here are primarily computational, with the stability equation expanded in a series with time-dependent coefficients. The solution methods, the limitations, and comparison of the two approaches are surveyed in the papers by Foster (1968), Robinson (1967) and Mahler *et al.* (1968).

For purposes of comparing analysis to experiment, linear theory has obvious limitations. The basic limitation is the identification of the onset of observable convection. That is, given an initial disturbance and its predicted growth, at what relative amplification is convection manifest? Strictly, observable motion is necessarily finite and therefore outside the range of linear theory. Also, there is the matter of specifying initial conditions. What are appropriate perturbations in terms of what can be realized experimentally? It was with these and other questions in mind that we set out to explore experimentally the onset problem.

Previous experimental studies have been mainly concerned with convection accompanying evaporation from an initially quiescent layer (Spangenberg & Rowland 1961; Foster 1965*b*). With evaporation the free surface boundary condition is somewhat difficult to control. That is, the upper surface of the evaporating liquid is cooled in some irregular, time-dependent manner determined by energy interchange between the liquid and the gas space above. Also, as with all free surface problems, there is the attendant difficulty of properly accounting for the rheological behaviour of the liquid surface itself. That is, with temperature-dependent surface tension the layer may be subject to surface-driven instabilities. Finally, for evaporation of water (both references above) the presence of trace quantities of surface-active impurities may have a pronounced effect on the evaporation rate. Because of these difficulties it was apparent that a non-evaporating system would be more amenable to quantitative study.

In previous work in this laboratory (Plevan & Quinn 1966) convection had been observed in an investigation of gas absorption into quiescent fluid layers. Here liquid density, which is concentration dependent, is changed by absorbing a soluble gas into the liquid. As opposed to evaporation, the surface boundary condition can be simply and reproducibly altered by changing the pressure of the pure absorbing gas. For a wide range of concentrations, liquid density is linearly dependent on concentration and, at the gas–liquid surface, the concentration of dissolved gas is linearly dependent on gas pressure (Henry's law). In the experiments described in this paper transient absorption was used to study the onset phenomena. Convection was initiated by imposing a step change in gas pressure. Growth of disturbances and patterns of motion were observed by measuring the rate of uptake of gas, the time-dependent surface flux, as well as viewing the layer in a schlieren optical system.

An additional advantage of controlling density by way of concentration is that gas–liquid pairs can be selected which are stable to surface-driven flows while

unstable to buoyancy drives (as well as the converse case) ensuring that only one type of instability is operative at onset. Experimental procedures are outlined in the next section followed by a discussion of our observations.

2. Experimental

The time of onset of convection was detected by two independent experimental methods. The first method consisted of continuously monitoring the rate of gas absorption into the liquid. Since convection augments transport into the liquid, the onset of convection is accompanied by a corresponding increase in the rate of absorption over that due to diffusion alone. The second method was a visual one in which onset was detected by viewing the liquid layer with schlieren optics. The time at which motion was first perceptible in the schlieren image was taken as the onset time.

Absorption measurements

The apparatus used to monitor the gas absorption rate was similar to that used by Plevan & Quinn (1966). Its essential components were: a high pressure reservoir of absorbing gas; two identical cells, one in which liquid was placed (the 'absorption cell'), the other an empty reference cell (the 'blank cell'); a bi-directional pressure transducer connected between the cells; a quick-acting valve with which the step-change in pressure was brought about. (The pressurization step by way of the quick-acting valve and high pressure reservoir differs from that of Plevan & Quinn who used a piston and cylinder device to change pressure abruptly.) The entire assembly was submerged in a constant temperature bath maintained at $24{\cdot}5 \pm 0{\cdot}01\,^{\circ}\mathrm{C}$.

The absorption cell was a 2 in. I.D. glass cylinder, 2 in. in height, held between two stainless-steel compression plates. The two cell arrangement (absorption plus blank cell) was used to subtract out the temperature effect caused by initial compression of the gas. Both cells had nearly identical thermal characteristics such that the temperature rise accompanying compression decayed with time in essentially the same manner in the two cells. After admitting high pressure gas simultaneously to both cells, valves were closed to isolate them from each other and from the high pressure reservoir. The signal recorded was the pressure difference between the two cells and, with the temperature effect counterbalanced, was caused solely by absorption into the liquid. It should be noted that the system pressure was essentially constant during the absorption period since the pressure decrease caused by absorption was very small relative to the absolute pressure. Also, small, thermally induced density gradients were present in the liquid because of the heat of solution accompanying the absorption. These heat effects were negligible in comparison to the density gradients resulting from concentration changes (Blair 1968).

Special care was taken to ensure that the liquid was at chemical equilibrium prior to a run and, also, that the system was free of any surface-active contaminants. Before an absorption experiment, all cell components contacting the absorbing liquid were cleaned in chromic acid. After the cell was assembled, the system was brought to thermal equilibrium and the cell was tested for leaks. Next,

25 cc of liquid presaturated with gas were injected into the absorption cell. The liquid in the cell was then stirred by means of a Teflon-coated magnetic stirring bar rotating at the bottom of the layer and powered by an external drive. Agitation was maintained for several hours, with continuous gas purging until complete equilibrium was attained. At this point mixing was stopped with the layer remaining quiescent for a period of several minutes before a convection experiment. For repeat runs, the liquid was stirred for at least one-half hour between experiments.

Schlieren system

For the visual studies a standard, two mirror schlieren apparatus was used. (A comprehensive discussion of schlieren methods and the interpretation of flow patterns in evaporating liquid layers as deduced from schlieren photography is

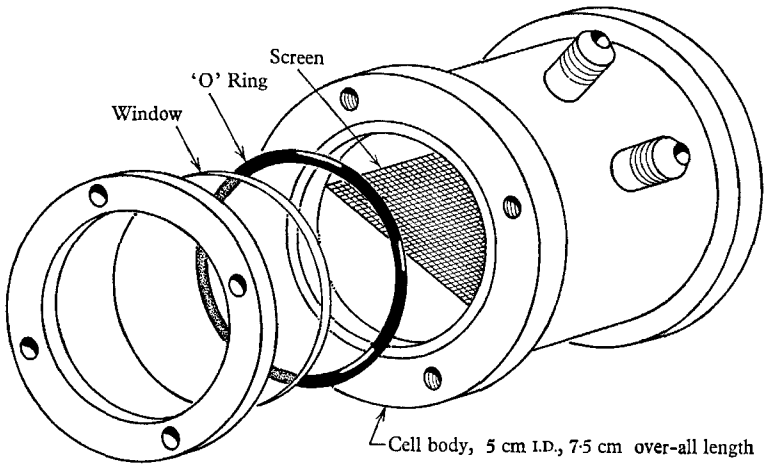

FIGURE 1. Optical cell.

contained in the recent paper of Berg, Boudart & Acrivos (1966).) Essentially, the schlieren method is a means by which refractive index gradients in a transparent medium can be made visible. A light ray passing through such a medium will be deflected by an amount proportional to the refractive index gradient normal to the path of the ray and the deflexion will be in the direction of maximum refractive index. With the limiting diaphragm, usually a straight edge, deflected rays either add to or subtract from the light normally present at the image plane of the schlieren field. The result is an image of light and dark areas for which points of equal brightness correspond to points of equal refractive index gradient. Since the refractive index is a function of liquid composition, images which we observed mapped out the concentration field in the convecting layer.

The collimating and schlieren mirrors, spaced 13 ft. apart, were a matched pair of parabolic front-surfaced mirrors, 6 in. in diameter with 4 ft. focal length. The light source was a 105 W, 6 V tungsten ribbon filament lamp and the limiting diaphragm was a blackened razor blade. For photography, a Bolex H16 reflex camera with Eastman Tri-X 7233 negative film was placed at the image plane.

The optical cell, i.e. the absorption cell used in all optical studies, is shown in figure 1. All metal parts, cell body, tubing connexions and pressure deflecting screen were stainless steel. The windows were optically-flat quartz disks, $2\frac{5}{8}$ in. diameter. Teflon or rubber 'O' rings were used in the seal between windows and cell body. To minimize initial disturbances a boss at the gas inlet deflected the entering gas stream parallel to the liquid interface and a 200-mesh screen placed across the diameter of the cell further dampened the initial pressure wave. Liquid depth was usually 1·5 cm with a magnetic stirring bar submerged in the liquid layer.

For viewing perpendicular to the liquid interface the cell was rotated 90° so that the axis of the cell was vertical. Four additional flat mirrors were then used to deflect the light beam through the cell without moving the basic components of the schlieren apparatus. No pressure deflecting screen was used with the cell in this position.

Equilibration and pressurization of the optical cell were similar to those of the absorption cell. However, in this case there was no blank cell or pressure transducer. Also, the optical cell was not placed in a constant temperature bath. Rather, the whole schlieren apparatus was set up in a constant temperature room maintained at $25 \pm 1\,^{\circ}\mathrm{C}$.

A complete discussion of all experimental details is to be found in Blair (1968).

3. Stability criteria

The basic equations of change which govern convection in layers such as those considered here are highly non-linear and before analytical deductions can be made a number of simplifying assumptions must be made. The mathematical model for the layer with linear density profile is summarized by Chandrasekhar (1961). Non-linear aspects of stability theory are discussed by Segel (1966) and the particular problem of the time-dependent density gradient is examined by Foster (1965*a*, 1968).

Independent of any particular model of the convection process some generalization of the stability criteria can be obtained from dimensional considerations alone. First, making the Boussinesq approximation (see Chandrasekhar) and using the linear equation of state, $\rho = \rho_0[1+\alpha(C-C_0)]$ where ρ is the liquid density, C is the solute concentration in the liquid and α is the concentration coefficient of expansion. The subscript zero refers to reference conditions, the reference state usually taken is that of the pure liquid. In addition, gas pressure and dissolved gas concentration are linearly related by an equation of the form $C = HP$, where H is a quasi Henry's law constant. Then reducing the equations to dimensionless form with the scale factors h for length, h^2/D for time and ΔC for concentration, where h is layer depth, D is solute diffusivity and ΔC is the concentration difference associated with the initial pressure change ΔP, two parameters appear: the Rayleigh number

$$R = g\alpha\Delta C h^3/D\nu, \tag{1}$$

where ν is the kinematic viscosity; the second group is the Schmidt number,

$S = \nu/D$. (For the analogous thermal problem D is replaced by thermal diffusivity κ and S by Prandtl number, $P = \nu/\kappa$.) The dimensionless time identified with the onset of convection is

$$\tau_c = (D/h^2)t_c, \tag{2}$$

where t_c is the dimensional onset time.

Throughout our experimental results layer depth is effectively semi-infinite, i.e. in all cases convection sets in before the time-dependent concentration profile reaches the layer bottom. Since we are dealing with maximum onset times of the order of 10^2 sec and liquid phase diffusivities of 10^{-5} cm^2/sec, the semi-infinite condition is fulfilled for layers greater than, say, 0·1 cm. For semi-infinite conditions, onset time must, obviously, be independent of layer depth. This deduction is consistent with the dimensionalization above only in the case that τ_c varies as the $-\frac{2}{3}$ power of the Rayleigh number, $\tau_c \sim R^{-2/3}$, a rearrangement of which gives the dimensional critical time in terms of pertinent measureable fluid properties as

$$t_c \sim [\nu/D^{1/2}\alpha H \Delta P]^{2/3}. \tag{3}$$

This relation may be viewed as a limiting condition which must be satisfied for buoyancy-driven convection in the limit of large layer depth.

An additional limiting condition forced by the nature of the experiment is that all experimental results are for large Schmidt number, greater than, approximately, 500. (In this limit of large Schmidt number, Foster's (1965*a*) analysis indicates that critical time is independent of Schmidt number and dependent on Rayleigh number alone.)

Besides t_c, onset should be characterized by a disturbance whose wavelength (λ_c) depends on the parameters governing system behaviour. If this disturbance size is expressed as a dimensionless horizontal wave-number $a = 2\pi h/\lambda$, then, as with t_c, for a semi-infinite layer h must disappear from all functional relations. This requires that a is proportional to $R^{1/3}$, or

$$\lambda_c \sim [D\nu/\alpha H \Delta P]^{1/3}. \tag{4}$$

If the convection is due to surface tension gradients rather than buoyancy forces then the stability analysis depends on surface properties. This mechanism is discussed by several authors, the papers by Sternling & Scriven (1964), Berg & Acrivos (1965), Scanlon & Segel (1967) and Vidal & Acrivos (1968) being particularly relevant to this work. Several parameters can enter into the stability analysis depending on the rheological properties used in describing the surface. For the simplest model of a non-deforming surface the system is governed by two groups: the Schmidt number and the Marangoni number, M, where

$$M = \sigma \Delta C h/\mu D \tag{5}$$

and σ is the concentration coefficient of surface tension, with surface tension assumed to vary linearly with concentration, and μ is liquid viscosity.

The Marangoni number is, therefore, the counterpart of the Rayleigh number for a surface-driven flow. For a semi-infinite layer, τ_c should be inversely proportional to the square of M, which yields

$$t_c \sim [\mu D^{1/2}/\sigma H \Delta P]^2. \tag{6}$$

Comparing (3) and (6) gives a convenient method for distinguishing surface and buoyancy-driven flows. These dimensional deductions are used in the subsequent section in reducing the experimental data.

4. Results and discussion

Time of onset

The identification of a fixed time, t_c, with the onset of convection involves some arbitrariness. Disturbances introduced at time zero follow some time course

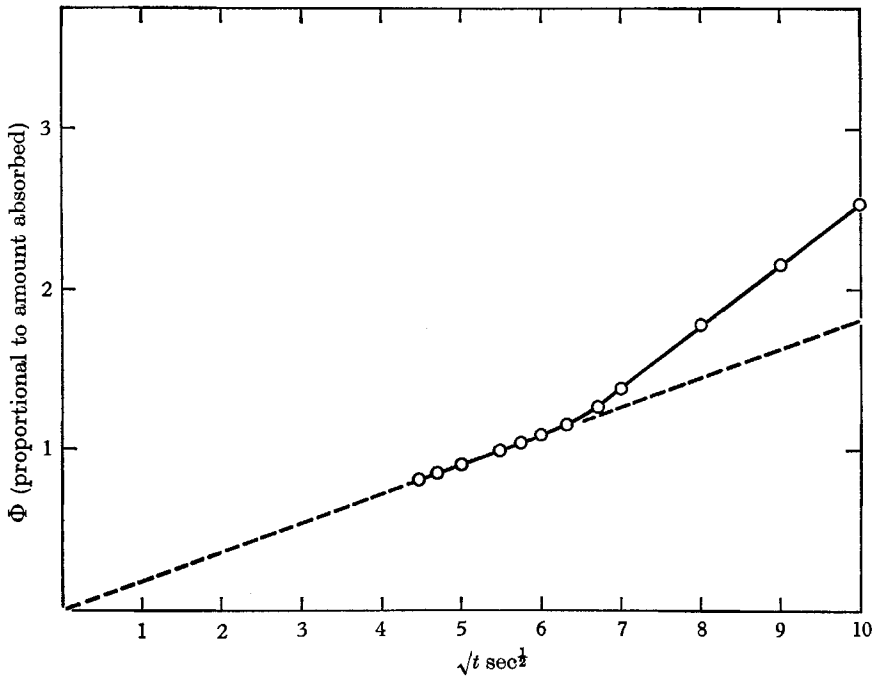

FIGURE 2. Total moles of gas absorbed as a function of $\sqrt{t}$.

(which may involve an initial period in which disturbances slowly decay, Mahler *et al.* 1968) such that their growth rate at the time at which motion is discernible is extremely rapid. The more sensitive the detection method, the smaller time at which growth can be observed. However, as explained below, since the time rate of change at onset is very large for large Rayleigh numbers, approaching exponential, it is unlikely that different detection methods will yield onset times which differ appreciably.

Typical results with the absorption cell are shown in figure 2 where the total amount of gas absorbed up to time t, Φ, is shown as a function of $\sqrt{t}$. For diffusion alone Φ is given by

$$\Phi = 2\Delta C \sqrt{(Dt/\pi)}.$$

For the data of figure 2, sulphur dioxide absorbing into an aqueous solution of sulphur dioxide at $\Delta P = 0{\cdot}08$ atm, Φ shows departure from molecular transport

at a time, t_c, of approximately 36 sec. Agreement between onset times measured in this manner and those measured in the optical cell is discussed in the next section.

Results for three gas–water pairs are shown on the logarithmic plot of figure 3. These particular gases, sulphur dioxide, ammonia and ethyl ether, were selected

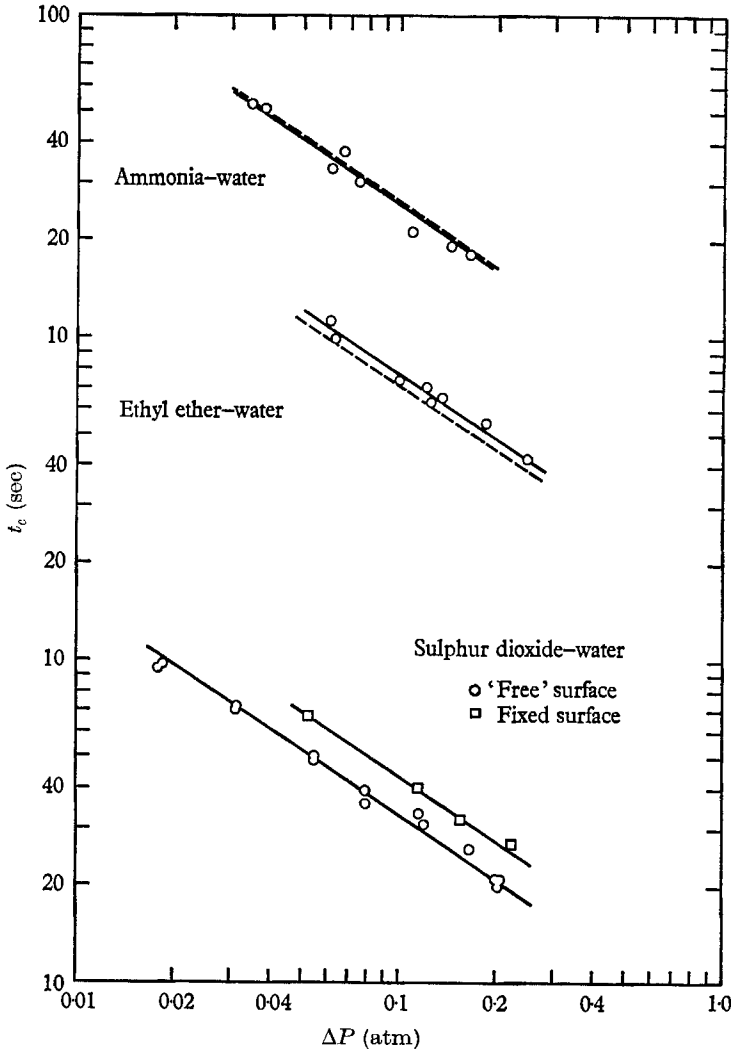

FIGURE 3. Time of onset of convection, t_c, as a function of initial pressure change, ΔP.

because of their high gas solubilities with the result that large density gradients were produced at relatively small values of ΔP. Throughout the experiments ΔP was selected to yield onsets of the order of 10–100 sec, a time sufficiently small to ensure that external conditions remained constant over the growth period.

A solution of sulphur dioxide in water is more dense than pure water, i.e. $\alpha > 0$.

For solutions of ammonia and of ethyl ether, $\alpha < 0$. Therefore, to initiate buoyancy-driven convection, sulphur dioxide was absorbed, the other two gases were desorbed in both cases giving a layer of heavier over lighter fluid. The sulphur dioxide data of figure 3 were obtained with the absorption cell, the other two curves were measured with the optical cell. The solid lines drawn through the points have a slope of $-\frac{2}{3}$, which, by (3), indicates a buoyancy mechanism for the instability.

Since the dynamical condition at the free surface can have a pronounced effect on the stability problem, this point was examined in some detail. To eliminate surface motion a 200 mesh (0·005 cm wire diameter) stainless-steel wire cloth was placed at the gas–liquid interface. Liquid wet the wire with the meniscus in the plane of the screen. With this configuration it can be assumed that the interface is *inflexible* and *laterally rigid*, a boundary condition comparable to that of a solid wall. Results for sulphur dioxide–water in the absorption cell with the screen in place are also shown in figure 3. Again, a slope of $-\frac{2}{3}$ is obtained but the magnitude of the onset times is increased over the previous results. An approximate calculation of the diminution in absorption rate caused by the screen shows that the two results are equivalent in terms of the total amount of gas absorbed. (The effect of the screen was not simply to reduce the absorption rate by an amount proportional to the fraction of the interface covered by the wire. Rather, the screen may be treated as a thin surface layer of smaller solute capacitance, smaller by the ratio of wire area to surface area, see Blair 1968.) This demonstrates that the condition of the free interface, i.e. without screen, is also equivalent to a laterally rigid, inflexible boundary. The conclusion to be made is that the water surface contains a surface-active contaminant capable of rendering the surface effectively rigid. Of course this surface rigidity applies only to the small motions prior to onset.

Recognizing that a water surface is 'inherently self-soiling' (Hickman 1952) and that trace quantities of surface-active materials are sufficient to yield a monomolecular surface layer of contaminant, the surface rigidity is not altogether surprising. Indeed, one can safely infer that a water surface with age greater than a few hours *is* contaminated, even though, as in these experiments, scrupulous attention was paid to cleanliness. The magnitude of this surface effect on the conditions for stability in the layer can be estimated from solutions to the Rayleigh problem for the case of a rigid boundary ($R_c = 1708$) as opposed to a free boundary ($R_c = 1100$) (Chandrasekhar 1961). It would appear that lateral rigidity may increase the critical Rayleigh number by as much as 50 %. Another conclusion to be drawn from the screen data is that since the fluid interface with wire cloth in place is inflexible and since the screen results agree with no-screen data, then the aqueous surfaces behave as inflexible boundaries, a condition of large surface tension. More details of the surface effect are discussed below.

Further verification of (3) was obtained by measuring t_c as a function of layer viscosity. Liquid viscosity was varied without significant change in other fluid properties by addition of small amounts of carboxymethylcellulose (CMC). In concentrations of 0·1–0·4 weight percent the CMC changed solution viscosity from 1 to 11 cp with negligible change in solute solubility or diffusivity. (This

interesting property of dilute aqueous gels was substantiated in previous experiments, Quinn & Blair (1967).)

Tests were made for sulphur dioxide absorbing into the gels in the absorption cell with wire cloth at the surface. Results are shown in figure 4 with the solid line through the data drawn with slope of $\frac{2}{3}$, the dimensional dependency as indicated in (3). Points at high viscosity deviate somewhat from the solid line. This may result from experimental error in viscosity measurement (a standard Ostwald viscometer was used with fluid taken from the cell at the end of an absorption run).

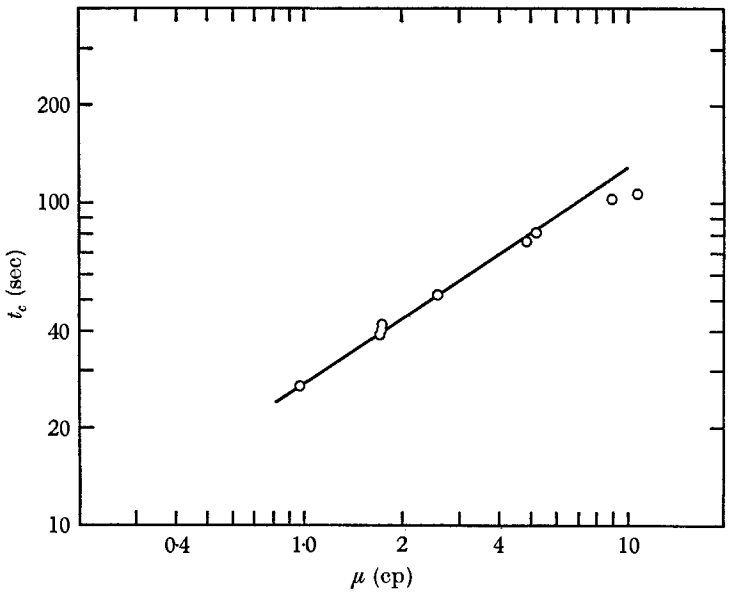

FIGURE 4. Time of onset of convection, t_c, as a function of layer viscosity, μ; sulphur dioxide–water system.

For an overall comparison of the onset data the results shown in figure 3 have been transformed to a consistent basis by means of the property values listed in table 1. The viscosities of the three systems were assumed equal; α for the sulphur dioxide–water system was measured in this laboratory (Blair & Quinn 1968), all other data were obtained from the literature. Note that the constants of table 1 apply only to the concentration range covered in our experiments. The dashed lines of figure 3 are the results predicted for ammonia–water and ethyl ether–water from sulphur dioxide onset data correcting for the appropriate physical constants by way of (3). Considering the precision of the property values, agreement among the results is impressive.

Therefore, the onset data may be summarized in one group and, for convenience, expressed as a critical value for a time-dependent Rayleigh number. Scaling with a length dimension appropriate to a semi-infinite layer, $\sqrt{(Dt)}$, the time-dependent critical Rayleigh number becomes

$$R_t = g\Delta\rho D^{1/2} t_c^{3/2}/\mu.$$

The buoyancy onset data for the three systems depicted in figure 3 are consistent with R_t having a numerical value of approximately 300. (The only additional aqueous system on which we have any onset results is carbon dioxide–water. Here, because of the lower solubility of carbon dioxide in water we were not able to operate in a pressure range which gave strong gradients of refractive index. The one measurement we do have, $\Delta P = 1$ atm with $t_c = 110$ sec, yields a value for R_t of about 200.) This value is, of course, a function of the particular initial disturbances present during our experiments and it is limited to large Schmidt numbers and to a rigid, conducting boundary.

System	α, g/g mole	$H \times 10^4$, g mole/g-atm	$D \times 10^5$, cm^2/sec
Sulphur dioxide–water	31·8[1]	12·9[1]	1·5[2]
Ammonia–water	5·1[3]	92[4]	2·3[5]
Ethyl ether–water	15[4]	1·2[4]	0·85[6]

[1] Blair & Quinn 1968.
[2] Plevan & Quinn 1966.
[3] *International Critical Tables.*
[4] Timmermanns 1959.
[5] Chiang & Toor 1964.
[6] Perry's *Chemical Engineer's Handbook*, 1903, 4th ed.

TABLE 1. Physical constants.

Form of motion

Flow patterns were viewed both parallel and perpendicular to the gas–liquid interface. Quantitative observations were limited to motion at onset, to buoyancy-driven flows and to a step-change initial condition. The sulphur dioxide–water system was susceptible to buoyancy convection alone whereas all other systems were susceptible to both buoyancy and surface tension convection. With ammonia–water and ethyl ether–water, surface contaminants apparently precluded surface-driven onsets; however, after onset there were indications that surface forces were exerting an influence on the form of motion. Because of the complexity of the combined buoyancy and surface flow, the remainder of this discussion is limited to the sulphur dioxide–water system.

For $\Delta\rho$ greater than approximately 0·003 g/cm^3 ($t_c < 40$ sec) motion appeared as a combination of rings, plunging columns or droplets, and sheet-like streamers. The first régime was caused by the meniscus at the cell walls (side view shown in figure 5, plate 1). Since the rate of absorption was uniform over the entire surface, the concentration boundary layer beneath the curved meniscus was effectively thicker than that under the flat surface and first motion occurred at the meniscus. Motion appeared as a plunging sheet of heavier fluid at the perimeter of the vessel. In figure 5 two plunging sheets are visible, one at each window of the optical cell.

The second régime, the true onset of convection, occurred in the form of rings with some plunging columns. Side and top views typical of this motion are shown in figures 6 and 8, plates 1 and 2 (pictures were not taken simultaneously but experimental conditions were identical). The rings broke from the surface region unevenly and as they plunged they tended to flatten out. The perpendicular view, figure 7, plate 1, shows their circular, crater-like shape; in the background

a network of less pronounced nodes can be seen between rings, these are the form of the third régime which follows. This stage of dense, plunging columns is shown in figure 7 in side view.

The diameter of these rings, taken as a horizontal length scale of onset motion, compares favourably with some predictions from linear stability theory as discussed below. The number of rings appearing at onset was not reproducible. In some runs several rings were visible; on a few occasions only columns were seen. The distance between columns was of the same order as the ring diameter.

As an example of the time scale involved, consider the sequence at $\Delta P = 0{\cdot}14$ atm ($\Delta\rho \sim 0{\cdot}006$ g/cm^3). The meniscus-induced plunging sheet occurred at about 20 sec (with negligible effect on absorption rate). Rings appeared in the interval of approximately 24–30 sec, with dense, columnar plunging following at approximately 30 sec. For these conditions t_c of 27 sec had been measured with the absorption cell.

For a comparison of the three gas–water systems, onset time, t_c, was taken to correspond to the first motion after the meniscus-induced sheet. No ambiguity existed for the ammonia–water and ethyl ether–water systems, onset motion was sudden and reproducible. However, for the sulphur dioxide–water system the time of appearance of first motion, i.e. the first ring, was somewhat inconsistent and was not accurately reproducible. When the onset time data measured in the absorption cell were compared with the two other systems, good agreement was obtained as indicated in figure 3, and this comparison was accepted. Relating the data in this manner introduced only small error. Had t_c been taken to be the inconsistent first ring onset, R_l would have been reduced to no less than 250 and, of course, agreement between the three systems would not have been quite as good.

For smaller driving forces, $t_c > 40$ sec, rings were not detected. Rather, first motion (following the meniscus effect) consisted of sheet plunging without the columnar mode. As time increased, the number of plunging sheets increased. In all cases after motion had penetrated to the bottom of the fluid layer a quasi-steady flow developed. The long-time flows displayed many of the characteristics noted by Berg *et al.* (1966) in a study of convection in evaporating layers.

Comparison with linear stability theory

The ring diameters measured as a function of ΔP for the onset patterns in the sulphur dioxide–water system are plotted in figure 9. The trend of the data agrees with the dimensional relation, equation (4). The two solid lines in figure 9 have been calculated from Foster's (1968) stability analysis. They represent predictions for the critical wave-number, i.e. the wave-number of the disturbance manifest at onset, for two different 'growth factors'.

The growth factor, $\overline{W}$, is a measure of the disturbance velocity. It is defined as the root mean square velocity at time t relative to that at time zero. Linear theory is incapable of predicting a particular growth factor at which convection is observable. However, Foster (1965*b*) has concluded that his experimental results on an evaporating water layer are consistent with previous experiments of Spangenberg & Rowland (1961) and that these results agree with his linear

analysis if onset is identified with a growth factor between one and two orders of magnitude. That is, the 'onset of instability' appears when initial disturbances have been amplified between 10 and 100 times.

The solid lines of figure 9 are for growth factors of 10^3 and 10^8, indicating that semi-quantitative agreement can be obtained over a wide range of amplification. It should be noted that disturbance wavelength is not a particularly sensitive

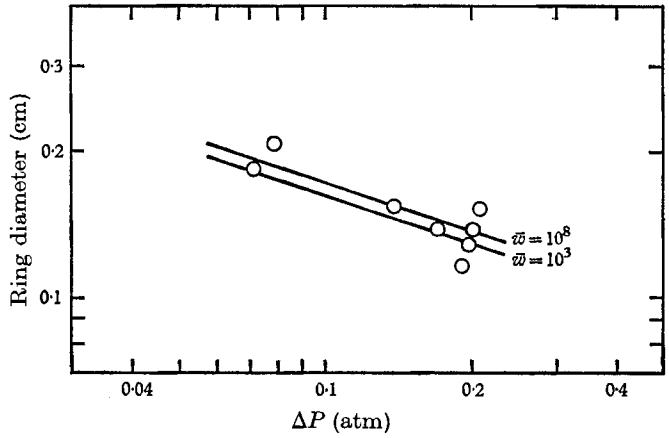

FIGURE 9. Ring diameter as a function of the initial pressure change, ΔP; sulphur dioxide–water system.

parameter of the growth factor. Moreover, at any particular t_c the range of measured wavelengths was large (of the order $\pm 20\,\%$). Foster (1965*a*) comments on these points: "The choice of the growth factor which defines the nominal critical time has only a slight influence on the determination of the critical wave-number. For a particular Rayleigh number the theory predicts that the disturbance which first manifests itself will have this critical wave-number. However, since the minima (in curves of t_c *vs.* a) are not sharply defined, it is evident that a range of wave-numbers will most likely be excited."

A more meaningful comparison of Foster's analysis with present results is in terms of the time-dependent Rayleigh number mentioned earlier in this discussion. The numerical value of 300 would call for a growth factor in the range of 6 to 7 orders of magnitude. [If the state of marginal stability, the point at which the layer is intrinsically unstable, is identified with the critical Rayleigh number, then Currie's (1967) analysis would predict a value of $\frac{1}{2}\pi^{3/2}$ or approximately 3 for R_t.] Note the linear theory is valid only for disturbances of infinitesimal amplitude and, strictly, observable motion is beyond the range of prediction. It is not obvious that relative amplitudes of 10^6 or greater can satisfy the infinitesimal criterion and retain physical meaning. However, it is possible that linear effects remain dominant long after the point at which the disturbances 'become finite'.

An important consideration in any time-dependent analysis is the selection of initial conditions. Although we did not have control over initial disturbances

in our experiments, it would appear that onset times were not particularly sensitive to the form of the starting perturbation. This is concluded on the basis of our nearly identical results with two different apparatus, with the optical cell in two different positions, and with the fine mesh screen placed directly at the fluid interface. In exploring this point, we performed a series of experiments with the optical cell in the horizontal position with the pressure deflecting screen removed from its normal position in the gas space. When high pressure gas was admitted to initiate a run, the surface was visibly deflected. Onset times were decreased from 20 sec with screen in place to approximately 18 sec with screen removed. With the optical cell in a vertical position no deflecting screen was used but significant differences in onset time were not detected. The precision of the vertical measurements was somewhat less than the horizontal ones and small differences, say 10 %, were within experimental error. This error was due to the difficulty in establishing first motion in a normal view of the interface. Apparently, widely variable initial conditions shifted onset times by no more than about 10 %.

Surface effects

The effect of surface tension gradients on the onset mechanism is minimized in the presence of surface contamination. For this reason, aqueous systems are dominated by buoyancy forces. To demonstrate surface-driven flows we, therefore, selected a binary organic solution with concentration-dependent density and surface tension. The system selected was ethyl ether-monochlorobenzene. Ether was desorbed from a solution containing 10 mole percent ether.

On desorption the solution is unstable to both buoyancy and surface tension mechanisms. Onset times measured in the optical cell are shown in figure 11. A surface free of contaminants gave times of 1·5 to 17 sec for ΔP of 0·1–0·02 atm. The best line through the data yields t_c varying as ΔP to the $-1{\cdot}8$ power as compared with $-2{\cdot}0$, as predicted for a surface driven flow, equation (6).

After these results were recorded, an organic surface-active agent was added to the solution. The substance added was dimethylpolysiloxane in a concentration less than 1 %. The change in convective behaviour is dramatic. Onset times shift by more than an order of magnitude and the $t_c - \Delta P$ dependency changes to the $-\frac{2}{3}$ power characteristic of the buoyancy-driven flow.

Unfortunately, we were not able to obtain accurate physical properties for the organic solution. A *very* approximate calculation using the buoyancy onset data yielded a value for R_l of the order of 10^3 (as opposed to 300 for the three aqueous systems). Whether the difference is real or due to errors in estimating α, D and H is unknown. The fact that the surface drive gives a ΔP dependency of $-1{\cdot}8$ rather than $-2{\cdot}0$ is not significant in light of experimental error. Also, it should be noted that the uncontaminated layer is susceptible to buoyancy as well as surface forces and, as shown by Nield (1964), at onset the driving force for motion is approximately the sum of the two.

A final noteworthy observation on surface effects is pictured in figure 10, plate 2. The view is normal to the interface of a 1 cm deep aqueous layer undergoing absorption of sulphur dioxide. The liquid in the lower half of the picture

was covered by a monomolecular layer of oleic acid, a typical long-chain surface active material. The upper half was covered by a layer of naturally present contaminant compressed by the oleic acid to a surface pressure of about 30 dynes/cm. This was accomplished by placing a small drop of oleic acid on the surface near the wall of the cell. The acid spread out compressing the contaminant to approximately one-half its original area. The schlieren image was then positioned to focus on the boundary region between the two surface films.

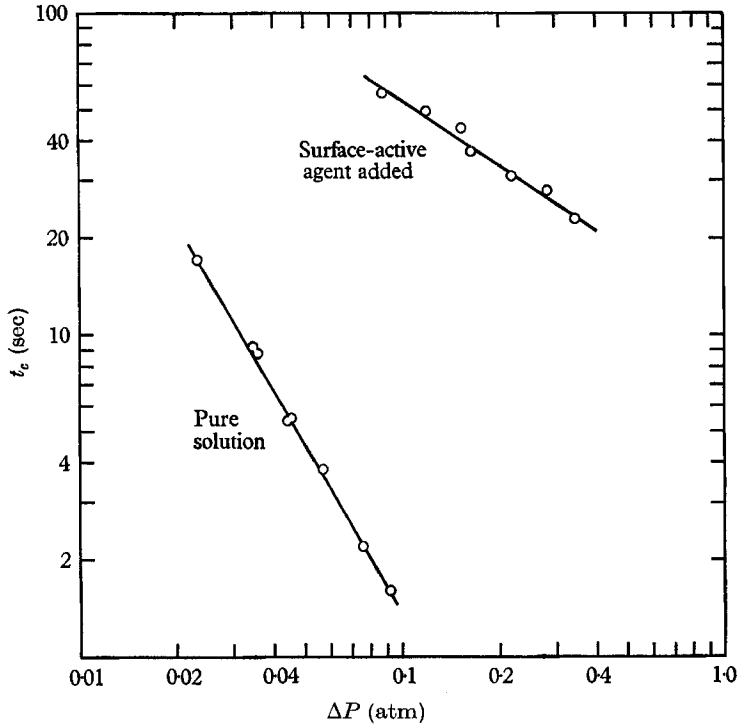

FIGURE 11. Time of onset of convection, t_c, as a function of initial pressure change, ΔP; ethyl ether–monochlorobenzene system.

As can be seen in figure 10 convection beneath the acid layer was well developed before motion set in under the compressed contaminant film. Onset time under the contaminant area was the same as in the absence of the oleic acid; onset under the acid covered area was about 4 sec earlier than the contaminant region. Since surface pressures, and therefore surface tensions, were the same over the entire surface and the contaminant onset was unaffected, the most likely explanation does not depend on surface flexibility. This follows from the fact that the wire cloth experiments showed that the aqueous surface was equivalent to an inflexible surface, i.e. one of high surface tension. On compression by the oleic acid, the surface tension was lowered but onset time remained substantially the same. That property of the two films which was different was their surface compressibility (Davies & Rideal 1961) and it is this property which would influence lateral rigidity. Apparently, the oleic acid film was more compressible than the

contaminant film, and for this reason onset first appeared under the acid. In viewing the motion it was also observed that the form of motion under the two regions was different. A detailed explanation would require more information on the contaminant film, information not easily obtained (see Merson & Quinn 1965).

This work was supported in part by a grant from the Office of Saline Water, U.S. Department of the Interior. The authors are grateful for this support as well as an American Oil Foundation Fellowship received by L. M. Blair.

REFERENCES

BERG, J. C. & ACRIVOS, A. 1965 *Chem. Engng. Sci.* **20**. 737.

BERG, J. C., BOUDART, M. & ACRIVOS, A. 1966 *J. Fluid Mech.* **24**, 721.

BLAIR, L. M. 1968 Ph.D. Thesis, University of Illinois, Urbana.

BLAIR, L. M. & QUINN, J. A. 1968 *Rev. Sci. Inst.* **39**, 75.

CHANDRASEKHAR, S. 1961 *Hydrodynamic and Hydromagnetic Stability*. Oxford: Clarendon Press.

CHIANG, S. H. & TOOR, H. L. 1964 *A.I.Ch.E.J.* **10**, 398.

CURRIE, I. G. 1967 *J. Fluid Mech.* **29**, 337.

DAVIES, J. T. & RIDEAL, E. K. 1961 *Interfacial Phenomena*. New York: Academic Press.

FOSTER, T. D. 1965*a* *Phys. Fluids*, **8**, 1249.

FOSTER, T. D. 1965*b* *Phys. Fluids*, **8**, 1770.

FOSTER, T. D. 1968 *Phys. Fluids*, **11**, 1257.

HICKMAN, K. C. D. 1952 *Ind. Engng. Chem.* **44**, 1892.

LICK, W. 1965 *J. Fluid Mech.* **21**, 565.

MAHLER, E. G., SCHECHTER, R. S. & WISSLER, E. H. 1968 *Phys. Fluids*, **11**, 1901.

MERSON, R. L. & QUINN, J. A. 1965 *A.I.Ch.E.J.* **11**, 391.

MORTON, B. R. 1957 *Quart. J. Mech. Appl. Math.* **10**, 433.

NIELD, D. A. 1964 *J. Fluid Mech.* **19**, 341.

PLEVAN, R. E. & QUINN, J. A. 1966 *A.I.Ch.E.J.* **12**, 894.

QUINN, J. A. & BLAIR, L. M. 1967 *Nature, Lond.* **214**, 907.

ROBINSON, L. 1967 *J. Fluid Mech.* **29**, 461.

SCANLON, J. W. & SEGEL, L. A. 1967 *J. Fluid Mech.* **30**, 149.

SEGEL, L. A. 1966 *Non-equilibrium Thermodynamics, Variational Techniques, and Stability*. University of Chicago Press.

SPANGENBERG, W. G. & ROWLAND, W. R. 1961 *Phys. Fluids*, **4**, 743.

STERNLING, C. V. & SCRIVEN, L. E. 1964 *J. Fluid Mech.* **19**, 321.

TIMMERMANNS, J. 1959 *Physico-Chemical Constants of Binary Systems*. New York: Interscience.

VIDAL, A. & ACRIVOS, A. 1968 *Ind. Engng. Chem. Fund.* **7**, 53.

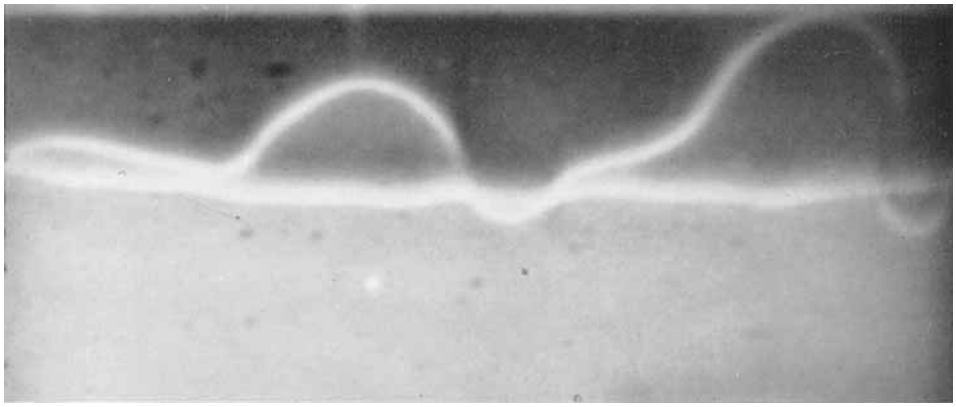

FIGURE 5. First régime.

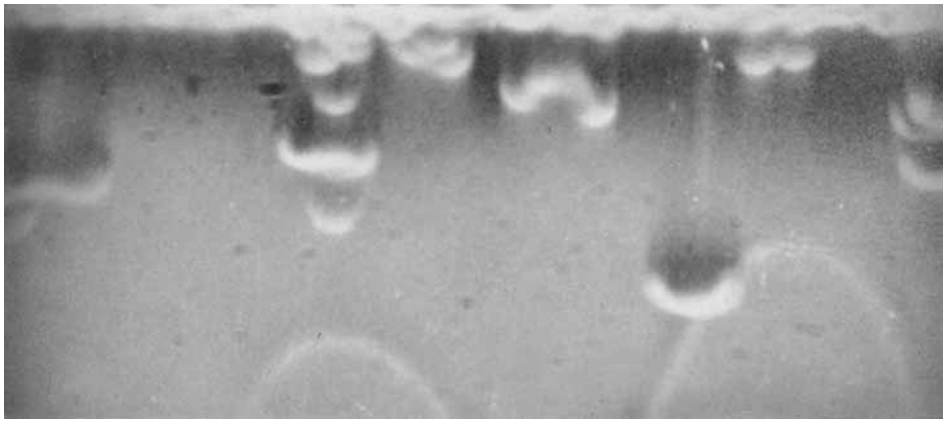

FIGURE 6. Second régime.

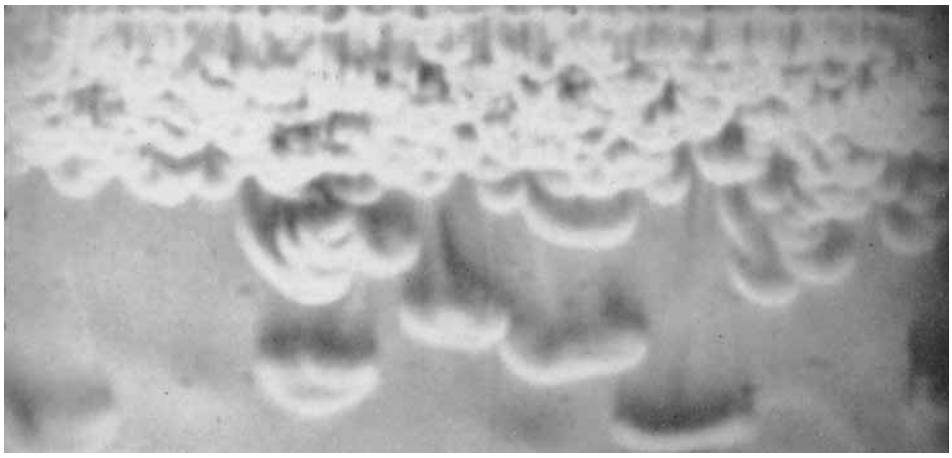

FIGURE 7. Third régime.

FIGURES 5–7. The three régimes of onset motion for sulphur dioxide–water system viewing parallel to the interface $\Delta P = 0{\cdot}18$ atm, field of view approximately 7×16 mm.

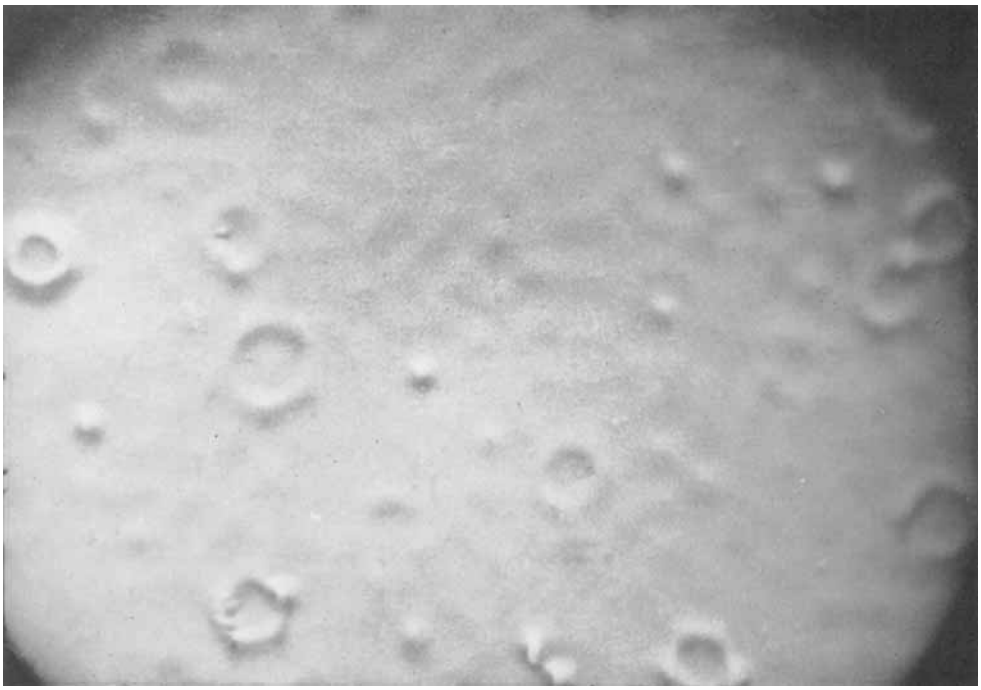

FIGURE 8. Second régime of onset motion for sulphur dioxide–water system viewing perpendicular to interface $\Delta P = 0{\cdot}18$ atm, field of view approximately 14×20 mm.

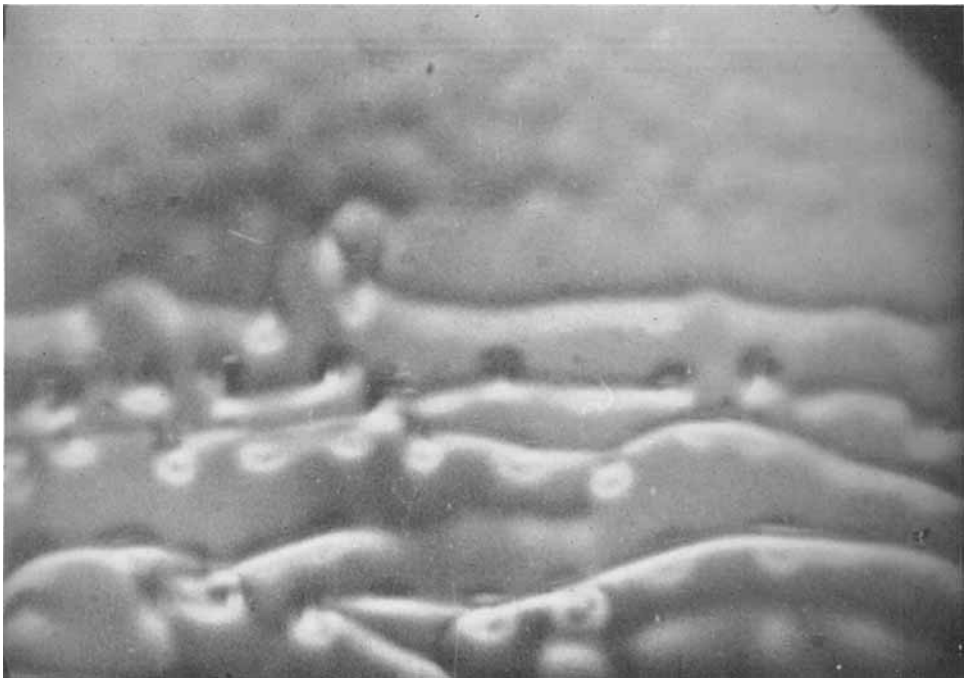

FIGURE 10. Sulphur dioxide–water system viewing perpendicular to interface. Surface of lower half of photograph covered by oleic acid monolayer, upper half by natural contaminant. $\Delta P = 0{\cdot}16$ atm, field of view approximately 14×20 mm.